Electronic Supplementary Information (ESI)

for

Isothermal titration microcalorimetry to determine the thermodynamics of metal ion removal by magnetic nanoparticle sorbents

Yuxiong Huang, Arturo A. Keller[*]

Bren School of Environmental Science and Management, University of California at Santa Barbara, CA, USA 93106

**Corresponding author*. Tel: +1 805 893 7548; fax: +1 805 893 7612. Email address: keller@bren.ucsb.edu

The SI contains 28 pages, 10 figures, and 4 tables.

1. Chemicals

Maghemite (iron (III) oxide) nanoparticles (30 nm in diameter), indium (III) chloride and pyridine were purchased from Alfa Aesar (USA). (3-aminopropyl)triethoxysilane (99%) were purchased from Sigma-Aldrich (USA). Cadmium chloride anhydrous, lead chloride, ethylenediaminetetraacetic acid (EDTA), sodium bicarbonate were purchased from Fisher Scientific (USA). Mercury (II) nitrate monohydrate, zinc (II) chloride, copper (II) chloride, gallium (III) chloride, cerium (III) chloride, chromium (III) chloride and diethylether were purchased from Acros Organics (Geel, Belgium). Toluene was purchased from EMD Millipore (USA). All chemicals were used as received, without further purification. All solutions were prepared with deionized water (18 MΩ-cm) from a Barnstead NANOpure Diamond Water Purification System (USA).

2. Synthesis of Mag-Ligand

Maghemite nanoparticles (1.0 g) were dispersed into 40 mL of toluene in a flask. After adding 0.4 mL of 3-aminopropyltriethoxysilane (APTES), the flask was connected to a reflux system (WU-28615-06, Cole-Parmer, USA), which was then rotated at 30 rpm (revolutions/minute) in a water bath at 90 ºC, and refluxed for 2 h. After the solution cooled to room temperature (22 ºC), 2 mM EDTA and 60 mL pyridine were added. The mixture was again rotated at 30 rpm in a water bath at 90 ºC in the reflux system for 2 h. After the solution cooled down to room temperature, 100 mL of sodium bicarbonate (0.5 M/L) was added to adjust pH. A magnet (Eclipse Magnetics N821 permanent, 50 mm

×50 mm ×12.5 mm; 243.8 g; pull force: 40.1 N) was applied to the bottom of the flask to recover the nanoparticles while the supernatant was decanted. Deionized (DI) water was used to rinse the particles twice and then decanted while retaining the particles with the magnet. The same rinsing procedure was performed twice with ethanol and then diethylether. The particles were dried at room temperature for 24 h, and stored in a capped bottle prior to use. The characterization of Mag-Ligand particles were reported in our previous study[1].

3. Characterization of Mag-Ligand

Transmission electron microscopy (TEM) images were obtained using a JEOL 1230 Transmission Electron Microscope operated at 80 kV. The thermogravimetric analyses (TGA) were used to investigate the amount of EDTA coated on the magnetic core, using a Mettler Toledo TGA/sDTA851e apparatus with an air flow of 100 mL/min and a heating rate of 5 °C/min. Magnetization measurements were performed on a Quantum Design MPMS 5XL SQUID Magnetometer. The functional groups of the Mag-Ligand composite were detected using a Fourier transform infrared (FTIR) spectrometer on a Nicolet iS 10 FT-IR Spectrometer.

The surface area of Mag-Ligands were determined using a computer-controlled nitrogen gas adsorption analyzer (TriStar 3000). Before measurements, the samples were degassed at 90 °C in a nitrogen flow for 12 h.

The zeta (ζ) potential (surface charge) of the Mag-Ligand was measured with a Zetasizer Nano-ZS90 (Malvern, UK) using folded capillary cells.

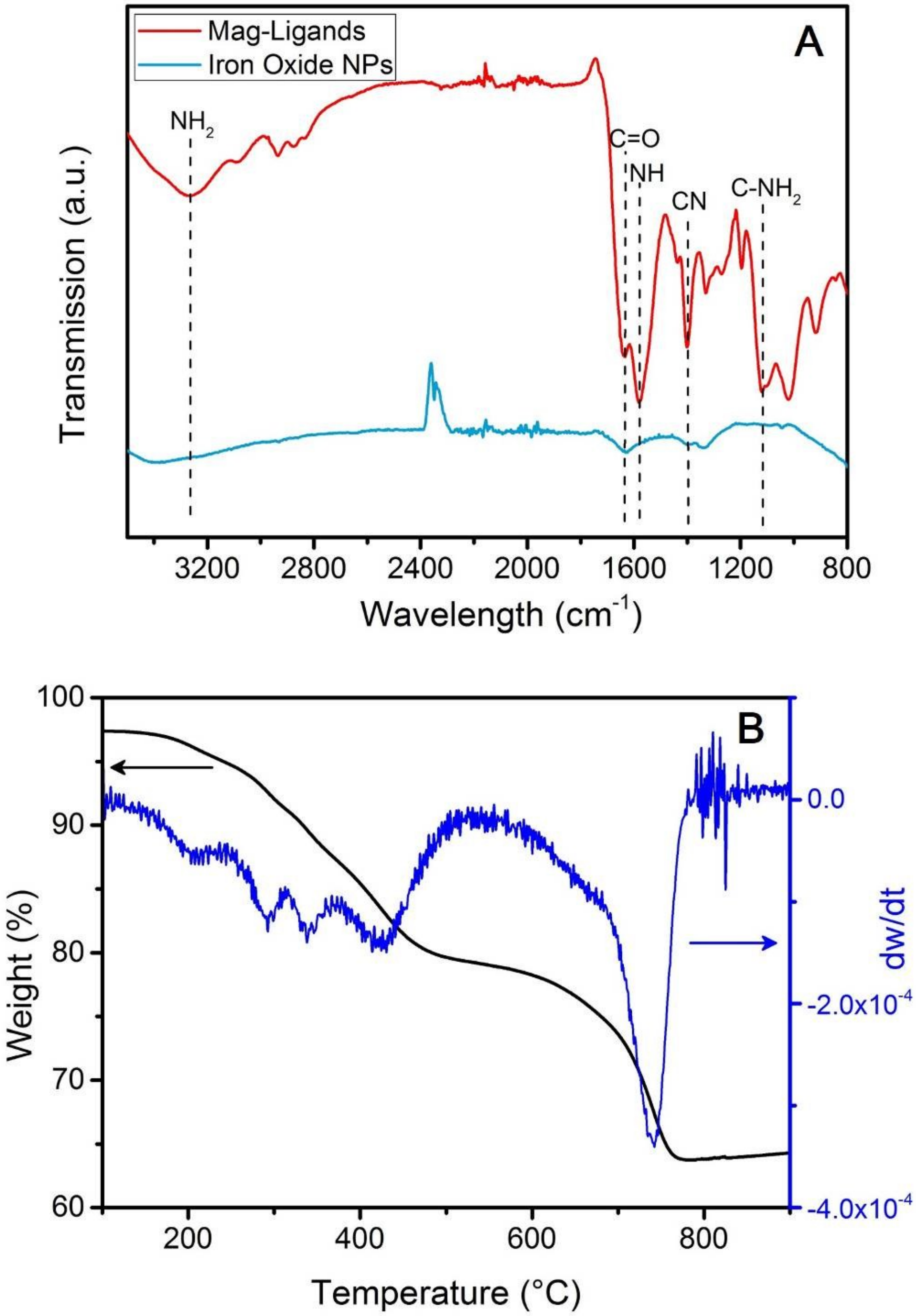

Figure S1. (A) FTIR spectra of unmodified magnetite nanoparticles and Mag-Ligand; (B) Thermogravimetric analysis (TGA) of Mag-Ligand.

The FTIR spectra of unmodified maghemite nanoparticles and Mag-Ligand are shown in Figure S1A. The Mag-Ligand presented peaks for N-H (v_{N-H}, 3267 cm^{-1}), C=O ($v_{C=O}$, 1633 cm^{-1}), N-H (v_{N-H}, 1580 cm^{-1}), C-N (v_{C-H}, 1400 cm^{-1}) and C-NH_2 (v_{C-H}, 1119 cm^{-1}); all these functional groups are expected from EDTA. These peaks were not present in the spectra of unmodified maghemite nanoparticles, indicating that the synthesis procedure had successfully attached EDTA on the surface of maghemite nanoparticles.

The TGA curves of as-synthesized Mag-Ligand (Figure S1B) show four weight loss steps at about 220, 292, 338, 424, and 742 °C, as demonstrated in the derivative curve, which can be ascribed to the decomposition of quaternary ammonium group[2], the decomposition of EDTA and transition from Na_2EDTA to Na_2CO_3, the decomposition of Na_2EDTA, and the complete oxidation of carbon, respectively[3]. The weight percentage of EDTA attached onto iron oxide particles of Mag-Ligand can be determined by the difference of initial and final mass of the sample in the TGA curve (Figure S1B) and was approximately 12.5% of the total mass of Mag-Ligand. The high fraction of EDTA and porous surface structure provides many active binding sites for metal ion removal.

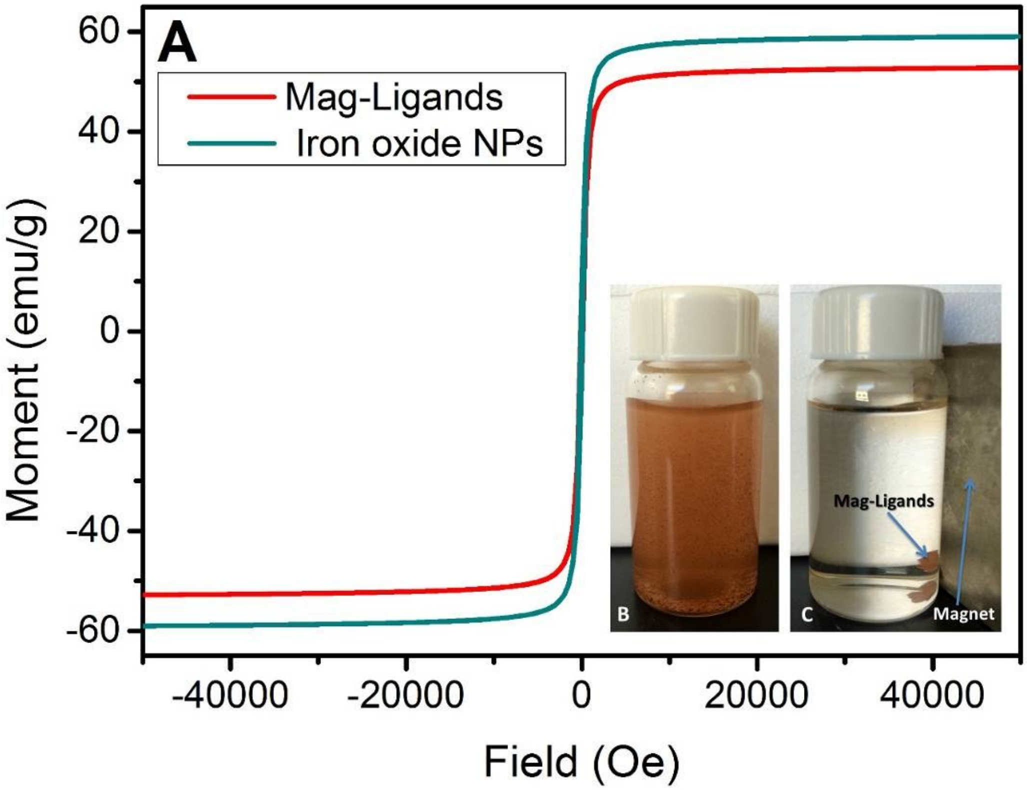

Figure S2. (A) The magnetic hysteresis loops of iron oxide nanoparticles and Mag-Ligand; (B) Mag-Ligand particles are introduced into a vial containing contaminated water; (C) A permanent magnet is placed at the side of the vial to attract the magnetic particles, demonstrating the rapid removal of Mag-Ligand from the suspension within seconds of applying a magnetic field.

Magnetic characterization with a superconducting quantum interference device (SQUID) magnetometer at 300 K indicated that maghemite and Mag-Ligand have magnetization saturation values of 59.0 and 52.8 emu/g, respectively (Figure S2A), indicating a high magnetization. The maghemite content in the macroporous composites is calculated to be as high as 35 weight %. Additionally, no remanence was detected in either maghemite or Mag-Ligand particles, indicating a superparamagnetism feature due to the nanosized maghemite. Due to the strong magnetization, Mag-Ligand suspended in water (0.2 g/L) can be quickly separated from the dispersion with a magnet (1000 Oe), as shown in Figure S2 B and C. These results indicate that the Mag-Ligand possesses excellent magnetic responsivity.

Table S1. Surface area and pore volume of Mag-Ligand

Surface Area (m^2/g)	Pore Volume (cm^3/g)
21.675	0.365

Figure S3 indicated the zeta (ζ) potential of Mag-Ligands as a function of pH. Each data point obtained with the Zetasizer was an average of three repetitions of 10 or more runs each. In the pH range 4-10, the surface charge of Mag-Ligand is negative.

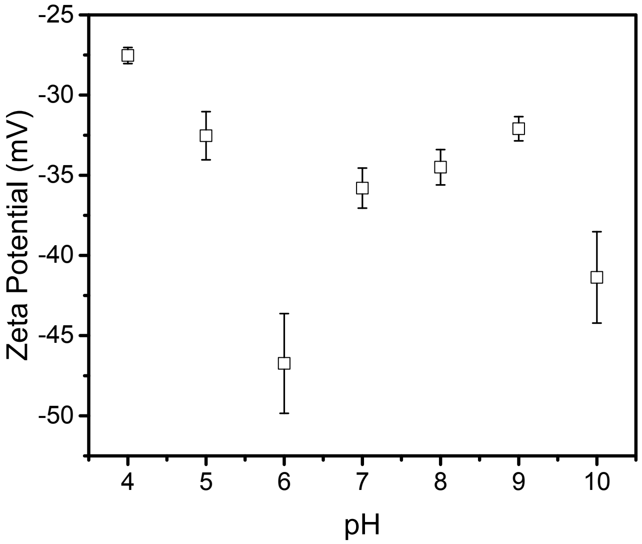

Figure S3. Mag-Ligand zeta potential as a function of pH.

4. Analysis

A Thermo iCAP 6300 inductively coupled plasma with atomic emission spectroscopy (ICP-AES) was used to analyze the concentration of metal ions. All tests were performed in triplicate and analysis of variance (ANOVA) was used to test the significance of results. A $p<0.05$ was considered to be statistically significant.

Metal ions removal efficiency and sorption capacity were calculated as:

$$Removal\ efficiency = \frac{C_0 - C_t}{C_0} \times 100\% \tag{S1}$$

$$Sorption\ capacity = q_e = \frac{(C_0 - C_t) \cdot V}{m} \tag{S2}$$

where C_0 and C_t are the initial and final concentrations of metal ions (mg/L), m is the mass of Mag-Ligand (g), and V is the volume of solution (L).

Mag-Ligand recovery efficiency was calculated as:

$$Recovery\ efficiency = \frac{C_w}{C_0} \times 100\%$$

(S3)

where C_0 (mg/L) is the initial concentrations of metal ions in solution, and C_w (mg/L) is the concentrations of metal ions in the extracted solution (after regeneration).

The metal ions equilibrium adsorption was evaluated according to Langmuir isotherms using Eq. 4, respectively [4]:

$$\frac{C_e}{q_e} = \frac{1}{K_L \cdot q_m} + \frac{C_e}{q_m}$$

(S4)

where C_e is solute concentration (mg/L) at equilibrium and q_e is amount adsorbed (mg/g), q_m is the maximum sorption capacity (mg/g). K_L is the Langmuir sorption equilibrium constant (L/mg).

Kinetics were analyzed using the pseudo-first-order and pseudo-second-order models using Eq. S5 and Eq. S6[5]:

$$\ln(q_e - q_t) = \ln(\mathrm{q}_e) - k_1 t$$

(S5)

$$\frac{t}{q_t} = \frac{1}{k_2 q_e^{\,2}} + \frac{1}{q_e} t$$

(S6)

where k_1 (h^{-1}) and k_2 $\left(\frac{g}{mg \cdot h}\right)$ are the equilibrium rate constant of kinetics.

5. Metal aqueous speciation

We used Visual MINTEQ model to simulate metal species distribution. In this pH range, metals are 100% dissolved. The metal aqueous speciation at pH 7 is listed in Table S2. Similar studies on Cd^{2+} were also reported in our previous paper [1]. From both studies, pH showed very minor effect on Mag-Ligand removal performance.

Table S2. Metal aqueous speciation at pH 7

Element	Species Name	% of total concentration
Cr^{3+}	$Cr(OH)_2^{1+}$	17.840
	$Cr_3(OH)_4^{5+}$	0.139
	$Cr_2(OH)_2^{4+}$	0.038
	$CrOH^{2+}$	3.474
	$Cr(OH)_3$ (aq)	78.505
Cu^{2+}	Cu^{2+}	22.645
	$Cu_2(OH)_2^{2+}$	28.405
	$Cu_3(OH)_4^{2+}$	42.353
	$CuOH^+$	6.461
	Cu_2OH^{3+}	0.021
	$Cu(OH)_2$ (aq)	0.115
Ce^{3+}	Ce^{3+}	96.906
	$CeOH^{2+}$	3.094
Zn^{2+}	Zn^{2+}	99.035
	$ZnOH^+$	0.860
	$Zn(OH)_2$ (aq)	0.104
In^{3+}	$In(OH)_2^+$	0.394
	$In(OH)_4^-$	0.200
	$In(OH)_3$ (aq)	99.406
Ga^{3+}	$Ga(OH)_4^-$	99.992
Hg^{2+}	$Hg(OH)_2$(aq)	99.994
Cd^{2+}	Cd^{2+}	99.930
	$CdOH^+$	0.069
Pb^{2+}	Pb^{2+}	78.779
	$Pb_3(OH)_4^{2+}$	1.311
	$Pb_4(OH)_4^{4+}$	1.994
	$PbOH^+$	17.343
	$Pb(OH)_2$ (aq)	0.053
	Pb_2OH^{3+}	0.521

In many cases the dominant species are free ions, such as Ce^{3+}, Zn^{2+}, Cd^{2+}, Pb^{2+}, and to make sure pH is consistent in all sorption studies, pH 7 was chosen as the condition to study. Though all the metals form aqueous hydroxide species at pH 7, but as the free ions bind to EDTA the equilibrium is driven towards more free ions.

6. Isothermal titration calorimetry measurement for nine different metal ions

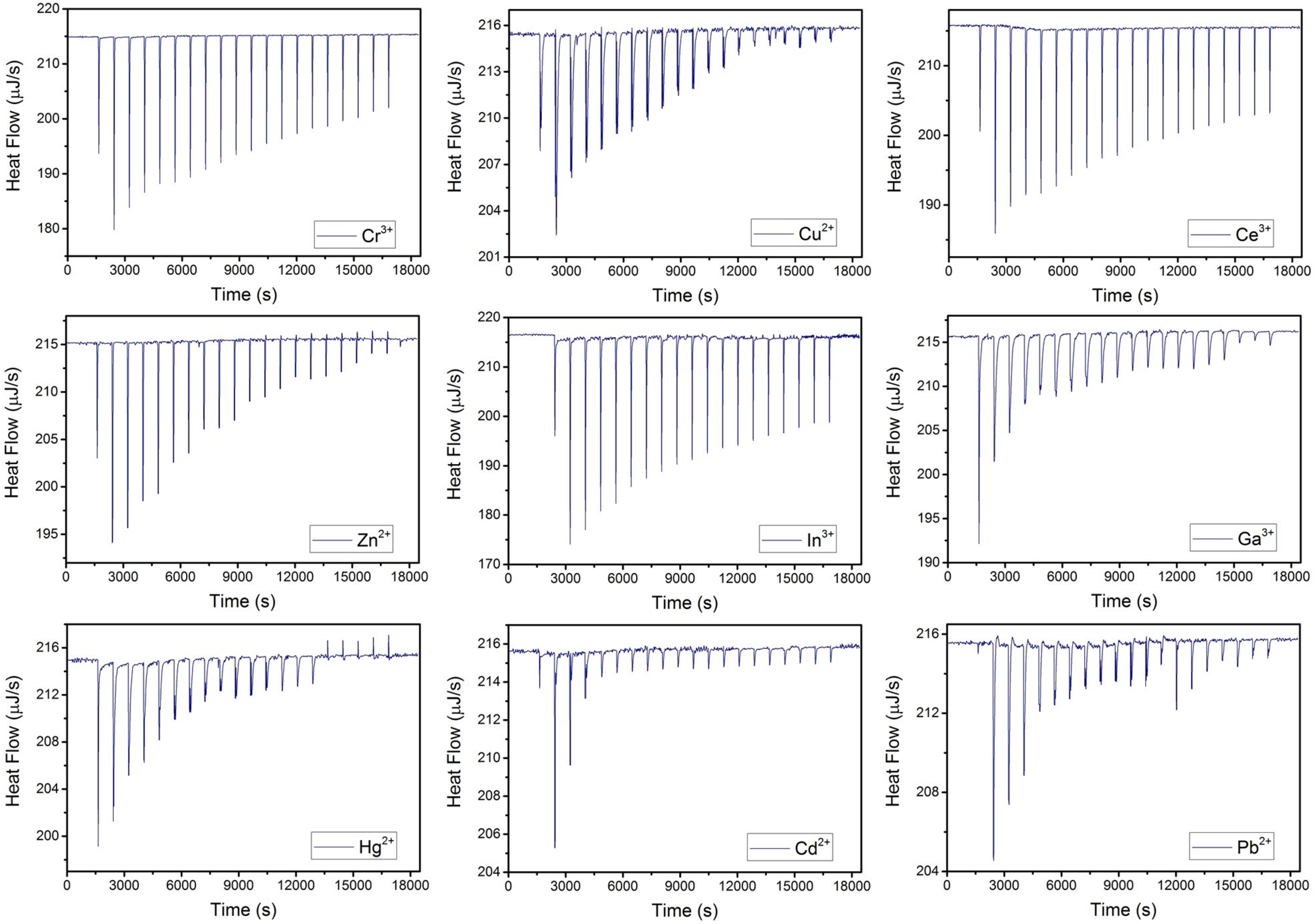
Heat Flow (μJ/s)
Time (s)
0
3000
6000
9000
12000
15000
18000
220
210
200
190
180
Cr^{3+}
216
213
210
207
204
201
Cu^{2+}
210
200
190
Ce^{3+}
215
210
205
200
195
Zn^{2+}
220
210
200
190
180
170
In^{3+}
215
210
205
200
195
190
Ga^{3+}
216
212
208
204
200
Hg^{2+}
216
214
212
210
208
206
204
Cd^{2+}
216
212
208
204
Pb^{2+}

Figure S4 Real-time thermogram for Mag-Ligand titration with nine different metal ions (Cr^{3+}, Cu^{2+}, Ce^{3+}, Zn^{2+}, In^{3+}, Ga^{3+}, Hg^{2+}, Cd^{2+} and Pb^{2+}) at 298 K.

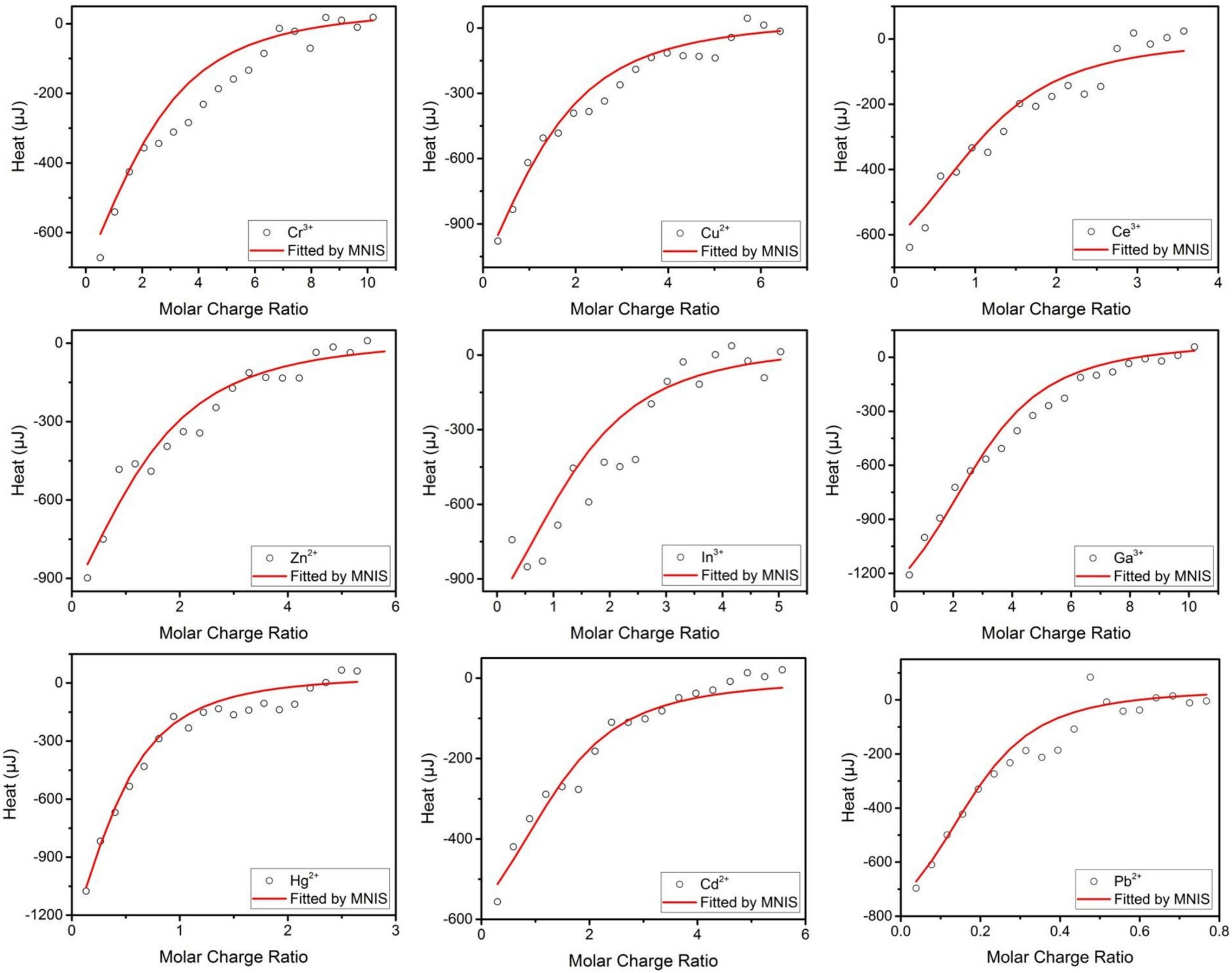
Heat (μJ)
Molar Charge Ratio
Cr3+
Fitted by MNIS
0
-200
-400
-600
0 2 4 6 8 10
Cu2+
Fitted by MNIS
0
-300
-600
-900
0 2 4 6
Ce3+
Fitted by MNIS
0
-200
-400
-600
0 1 2 3 4
Zn2+
Fitted by MNIS
0
-300
-600
-900
0 2 4 6
In3+
Fitted by MNIS
0
-300
-600
-900
0 1 2 3 4 5
Ga3+
Fitted by MNIS
0
-300
-600
-900
-1200
0 2 4 6 8 10
Hg2+
Fitted by MNIS
0
-300
-600
-900
-1200
0 1 2 3
Cd2+
Fitted by MNIS
0
-200
-400
-600
0 2 4 6
Pb2+
Fitted by MNIS
0
-200
-400
-600
-800
0.0 0.2 0.4 0.6 0.8

Figure S5 The integrated binding isotherms as a function of molar charge ratio of metal ions (Cr^{3+}, Cu^{2+}, Ce^{3+}, Zn^{2+}, In^{3+}, Ga^{3+}, Hg^{2+}, Cd^{2+} and Pb^{2+}) to Mag-Ligand particles were fitted with independent model, symbols represent experimental data, and red line represents model prediction

7. Individual sorption capacity

The specific BET surface area of Mag-Ligands is 21.68 m^2/g. The isotherm non-competitive sorption for each metal ion (Cr^{3+}, Cu^{2+}, Ce^{3+}, Zn^{2+}, In^{3+}, Ga^{3+}, Hg^{2+}, Cd^{2+} and Pb^{2+}) was studied, and the data was analyzed with Langmuir isotherm model. The predicted sorption capacity (mg/m^2) of each metal ion was listed in Table S3.

Table S3. Langmuir isotherm model predicted sorption capacity of each individual metal ion onto Mag-Ligand

Element	Sorption Capacity (mg/m^2)
Cr^{3+}	0.838
Cu^{2+}	1.07
Zn^{2+}	1.54
In^{3+}	1.58
Ga^{3+}	1.70
Ce^{3+}	1.27
Cd^{2+}	3.66
Hg^{2+}	3.46
Pb^{2+}	5.18

8. Sorption kinetics of individual metal ions

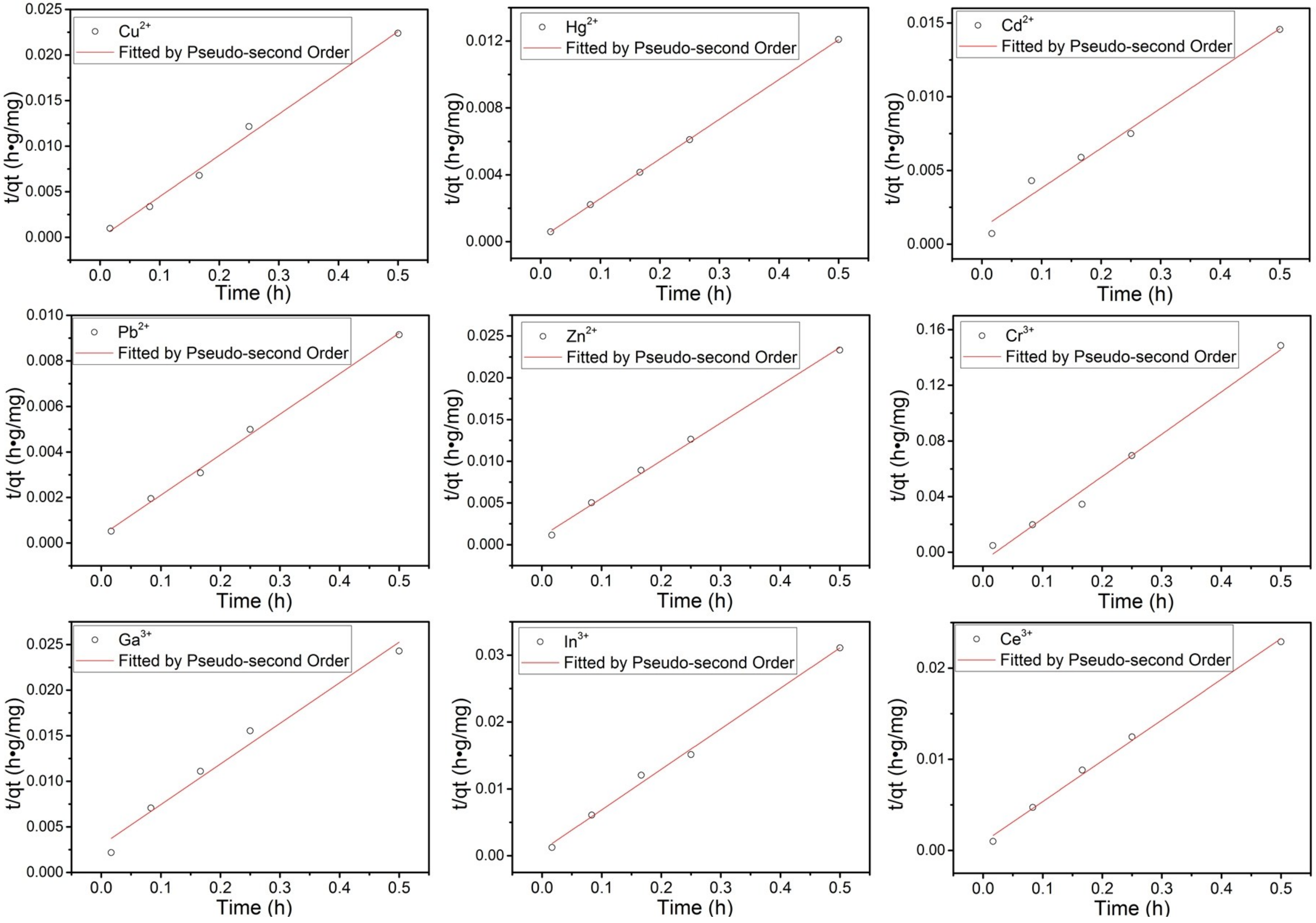
Cu^2+
Fitted by Pseudo-second Order
t/qt (h•g/mg)
0.000
0.005
0.010
0.015
0.020
0.025
Time (h)
0.0
0.1
0.2
0.3
0.4
0.5
Hg^2+
Fitted by Pseudo-second Order
t/qt (h•g/mg)
0.000
0.004
0.008
0.012
Time (h)
Cd^2+
Fitted by Pseudo-second Order
t/qt (h•g/mg)
0.000
0.005
0.010
0.015
Time (h)
Pb^2+
Fitted by Pseudo-second Order
t/qt (h•g/mg)
0.000
0.002
0.004
0.006
0.008
0.010
Time (h)
Zn^2+
Fitted by Pseudo-second Order
t/qt (h•g/mg)
0.000
0.005
0.010
0.015
0.020
0.025
Time (h)
Cr^3+
Fitted by Pseudo-second Order
t/qt (h•g/mg)
0.00
0.04
0.08
0.12
0.16
Time (h)
Ga^3+
Fitted by Pseudo-second Order
t/qt (h•g/mg)
0.000
0.005
0.010
0.015
0.020
0.025
Time (h)
In^3+
Fitted by Pseudo-second Order
t/qt (h•g/mg)
0.00
0.01
0.02
0.03
Time (h)
Ce^3+
Fitted by Pseudo-second Order
t/qt (h•g/mg)
0.00
0.01
0.02
Time (h)

Figure S6 Individual metal ions (Cu2+, Hg2+, Cd2+, Pb2+, Zn2+, Cr3+, Ga3+, In3+ and Ce3+) sorption kinetics fitted by Pseudo-second order onto Mag-Ligand in solution at pH 7.

9. Effect of pH on Pb^{2+} removal

Adsorption of Pb^{2+} onto Mag-Ligand was also performed at various solution pH. The pH was varied from 4 to 7, and pH was adjusted by using 0.1 M NaOH and HCl. Pb^{2+} was selected as an example to study the influence of pH on the removal efficiency, given its high abundance in waste water. The removal efficiency was found to decrease gradually as pH increased between pH 3 and 7, while the sorption capacity stabilized at around 50 mg/g at the range of pH 3 to 6 (Figure S7). This is not due to a decrease in affinity, but rather a change in Pb^{2+} speciation. Based on the simulation of lead species using Visual MINTEQ[6] software, the main Pb species present in the pH range 3 to 6 is Pb^{2+}, while the formation of solid $Pb(OH)_2$ starts at pH 6.3 and $PbOH^{3-}$ dominates above pH 7.0 [7]. Pb^{2+} has a strong complex formation constant with EDTA (at 25ºC log K=18.04)[8], which agrees well with our result: Mag-Ligand showed high sorption capacity across different pH, especially from pH 3 to 6.

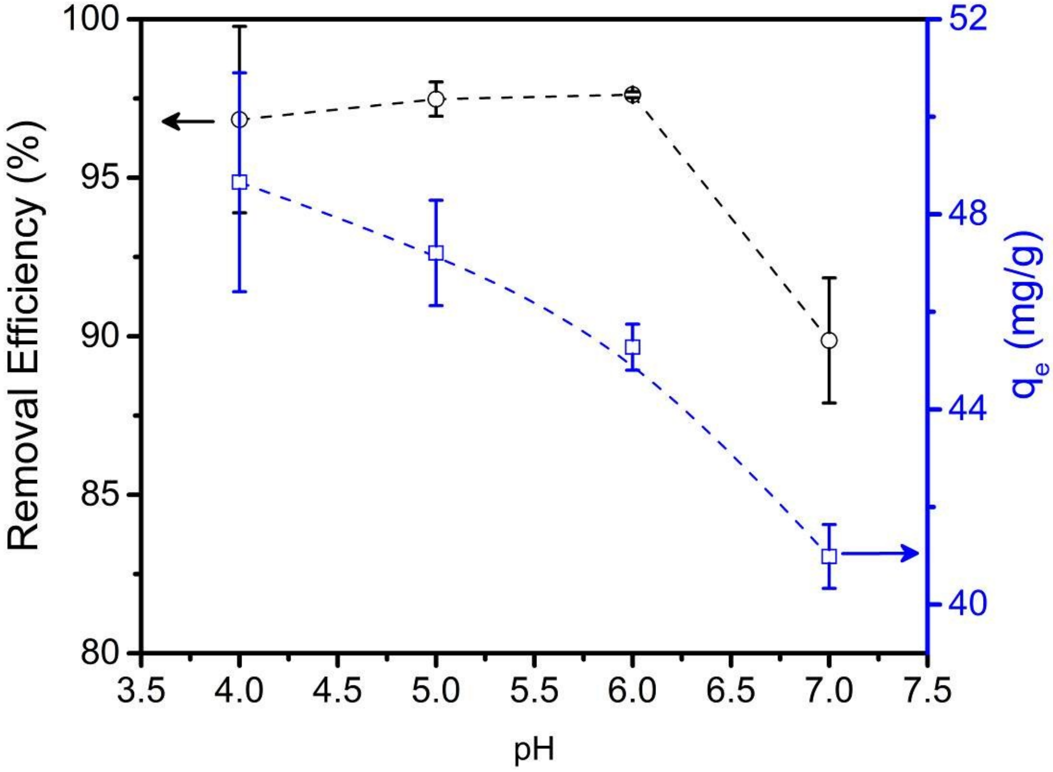

Figure S7 Adsorption of Pb^{2+} onto Mag-Ligand in solution as a function of pH, characterized by the removal efficiency (○) and adsorption capacity (□).

10. Effect of water hardness on Pb^{2+} removal

Water hardness, usually expressed as the total amount of Ca^{2+} and Mg^{2+} present in the water, varies in different water matrices, and both Ca^{2+} and Mg^{2+} can also interact with EDTA to form complexes[9]. In order to study the effect of ionic strength, especially water hardness, on the removal efficiency of Mag-Ligand on metal ions, two different common ions, Ca^{2+} and Mg^{2+} were used at concentrations ranging from 1 mg/L to 100 mg/L. The experiments were done as described earlier at pH 7.

Figure S8 shows the remediation performance of Pb^{2+} as a representative metal ion by Mag-Ligand in the presence of different concentrations of Ca^{2+} or Mg^{2+}. No significant difference in Pb^{2+} removal efficiency was found as Mg^{2+} or Ca^{2+}concentration increased up to 100 mg/L in solution (Figure S8). These results indicate that Ca^{2+} or Mg^{2+} did not compete strongly with Pb^{2+} in the complexation reaction with EDTA due to relative low complex formation constants between Ca^{2+} or Mg^{2+} and EDTA (log K is 8.79 for Ca^{2+} and 10.69 for Mg^{2+} at 25 °C) [8].

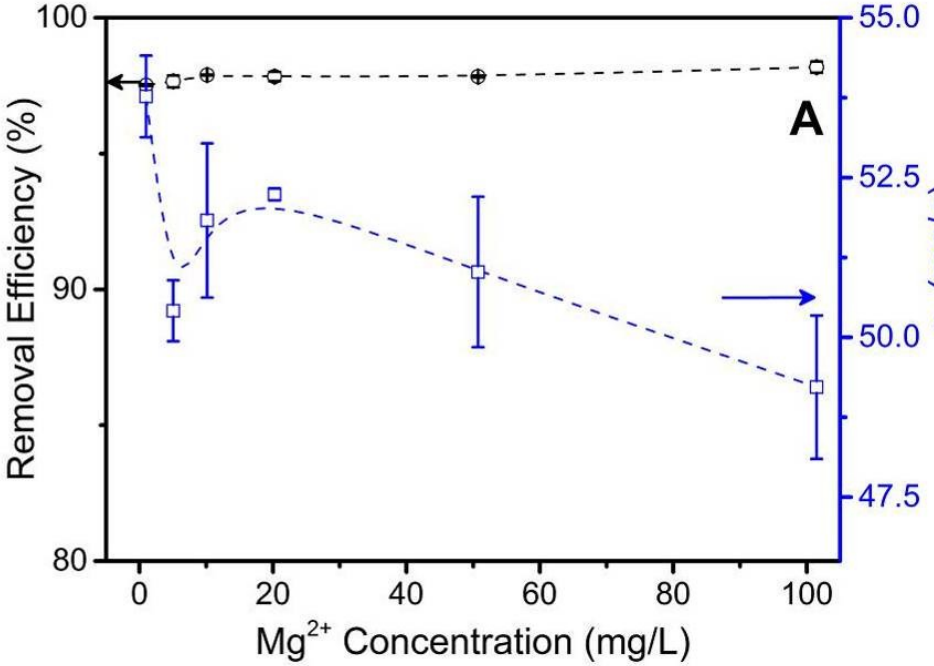

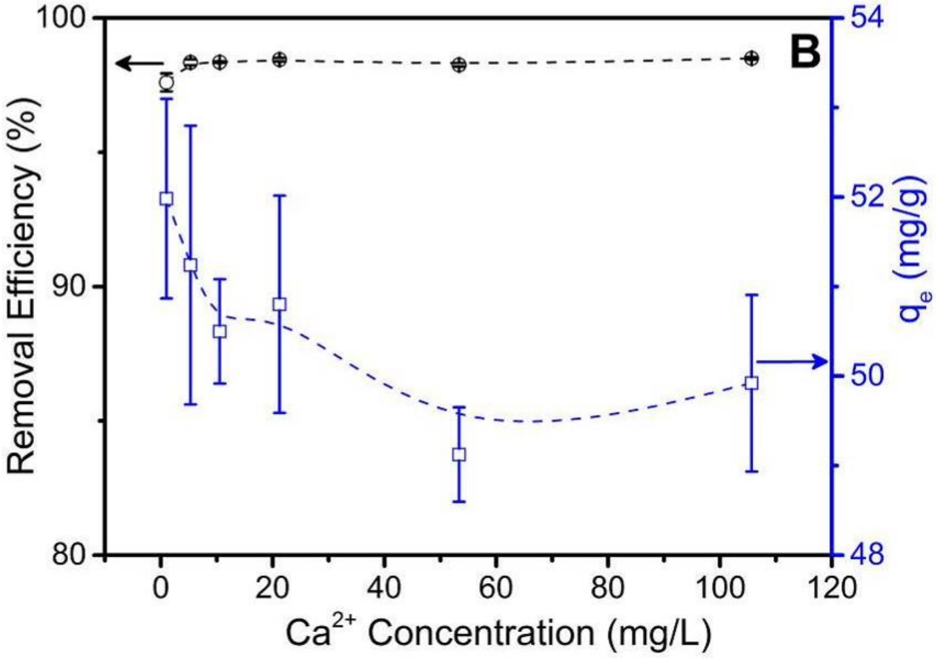

Figure S8 Adsorption of Pb^{2+} (10 mg/L initial concentration) onto Mag-Ligand (removal efficiency (○) and adsorption capacity (□)) in the presence of (A) Mg^{2+} (from 1 mg/L to 100 mg/L) and (B) Ca^{2+} (from 1 mg/L to 100 mg/L) at pH 7.

11. Competitive sorption of multiple metal ions

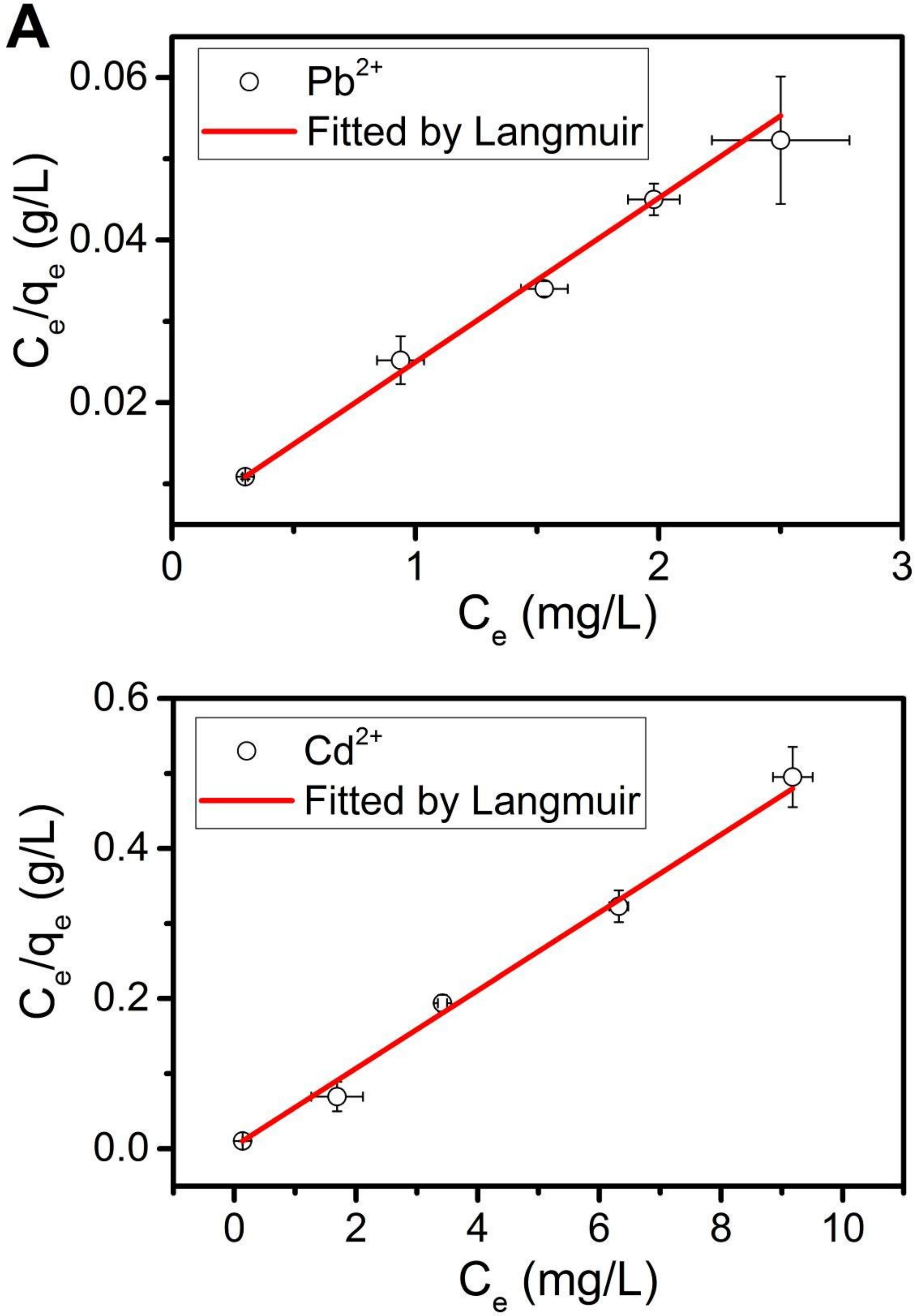
A
Pb^{2+}
Fitted by Langmuir
0.06
0.04
0.02
C_e/q_e (g/L)
0
1
2
3
C_e (mg/L)
Cd^{2+}
Fitted by Langmuir
0.6
0.4
0.2
0.0
C_e/q_e (g/L)
0
2
4
6
8
10
C_e (mg/L)

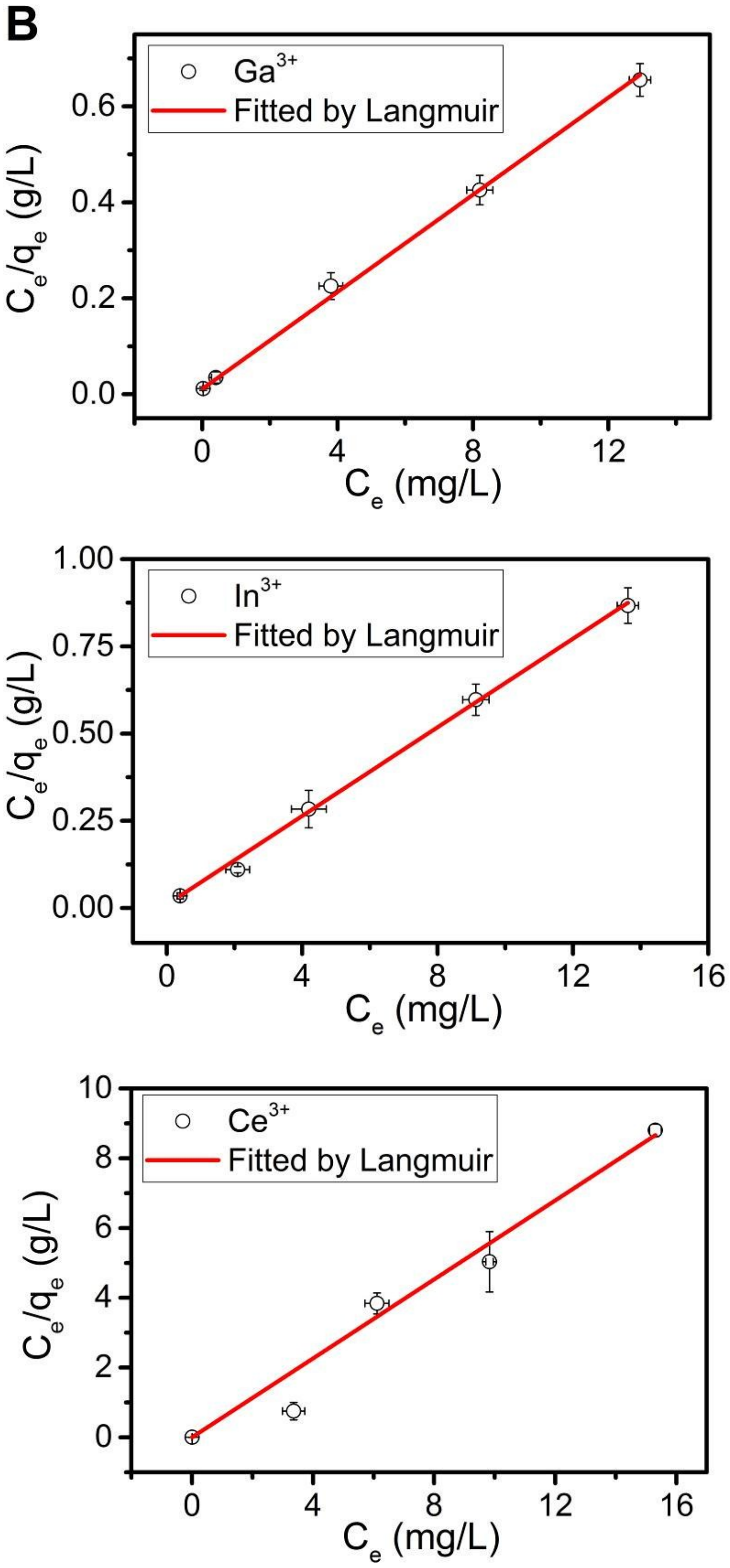
B
Ga^{3+}
Fitted by Langmuir
C_e/q_e (g/L)
0.0
0.2
0.4
0.6
0
4
8
12
C_e (mg/L)
In^{3+}
Fitted by Langmuir
C_e/q_e (g/L)
0.00
0.25
0.50
0.75
1.00
0
4
8
12
16
C_e (mg/L)
Ce^{3+}
Fitted by Langmuir
C_e/q_e (g/L)
0
2
4
6
8
10
0
4
8
12
16
C_e (mg/L)

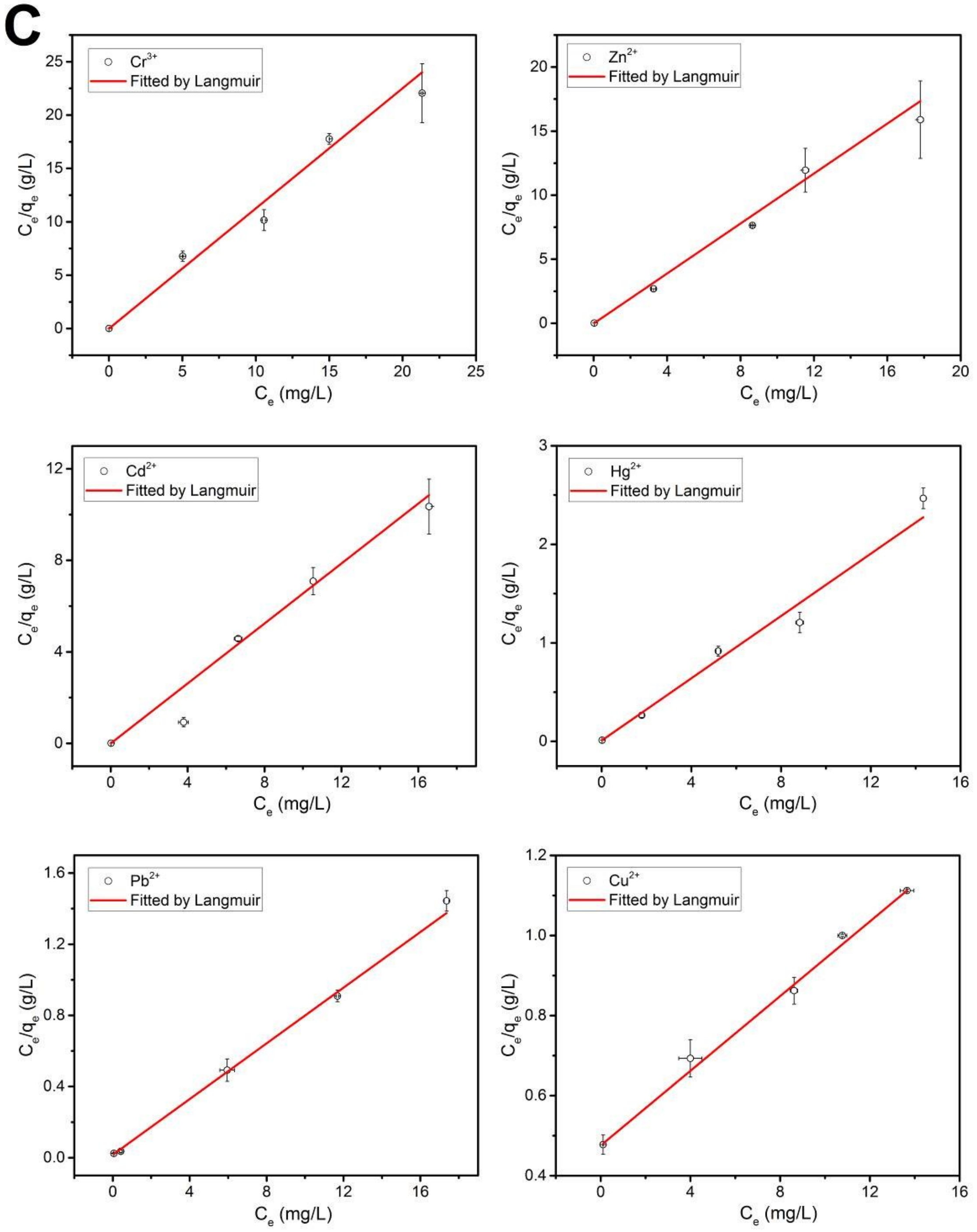

Figure S9 Competitive sorption of multiple metal ions fitted by Langmuir adsorption isotherms model: (A) Group 1: Cd^{2+} and Pb^{2+}; (B) Group 2: Ce^{3+} In^{3+} and Ga^{3+}; and (C)

Group 3: Cr^{3+}, Zn^{2+}, Cd^{2+}, Hg^{2+}, Pb^{2+} and Cu^{2+} at pH 7, symbols represent experimental data, and red line represents model prediction.

Table S4. Langmuir isotherm model fitted parameters for each metal ion in group competitive sorption onto Mag-Ligand

	Element	q_m (mg/g)	K_L (L/mg)	R^2
Group 1	Cd^{2+}	19.25	16.59	0.996
	Pb^{2+}	49.55	4.187	0.996
Group 2	Ce^{3+}	1.767	-393.0	0.996
	In^{3+}	15.75	6.335	1.000
	Ga^{3+}	19.76	4.592	0.999
Group3	Cr^{3+}	0.888	-113.61	0.988
	Zn^{2+}	1.025	-39.00	0.997
	Cd^{2+}	2.073	-72.54	0.999
	Hg^{2+}	6.326	20.40	0.995
	Pb^{2+}	12.78	4.846	0.997
	Cu^{2+}	21.44	0.098	1.000

12. Equi-molar competitive adsorption for multiple metal ions

As the molar weight of different metal ions varies, we also conducted equi-molar competitive adsorption, shown as Figure S10. The results are very similar to the equi-mass competitive adsorption (Figure 6), especially in Group 3, Cu^{2+} had the higher removal efficiency than other metal ions at the higher initial concentration (Figure S10C).

The results suggested the adsorption kinetic rate as well as the binding affinity dominate competitive adsorption of multiple metal ions.

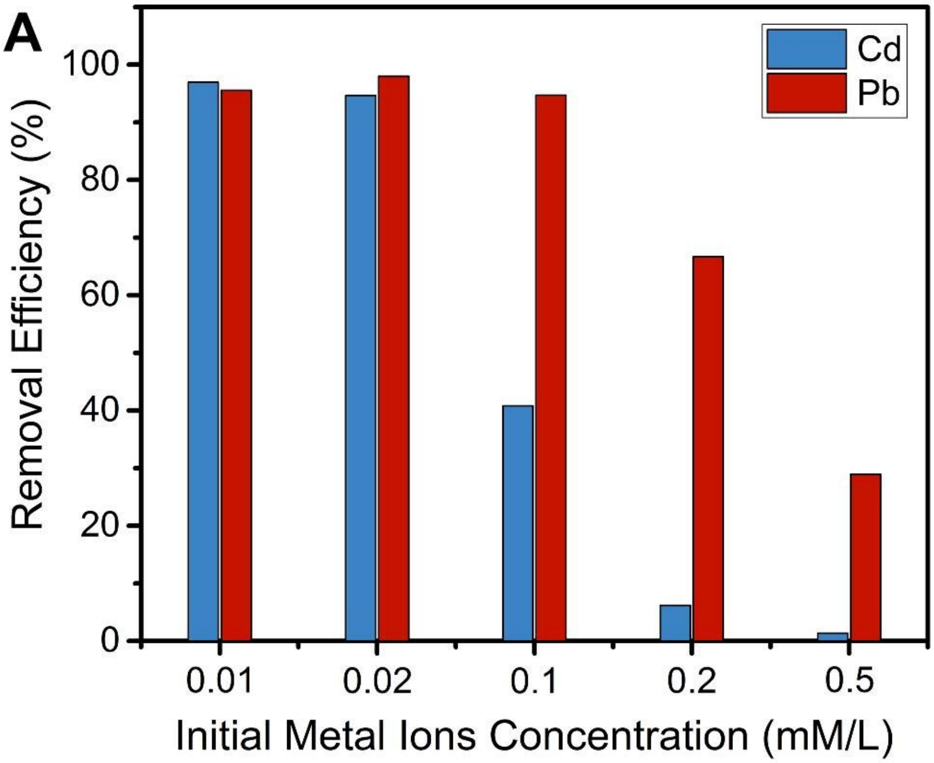

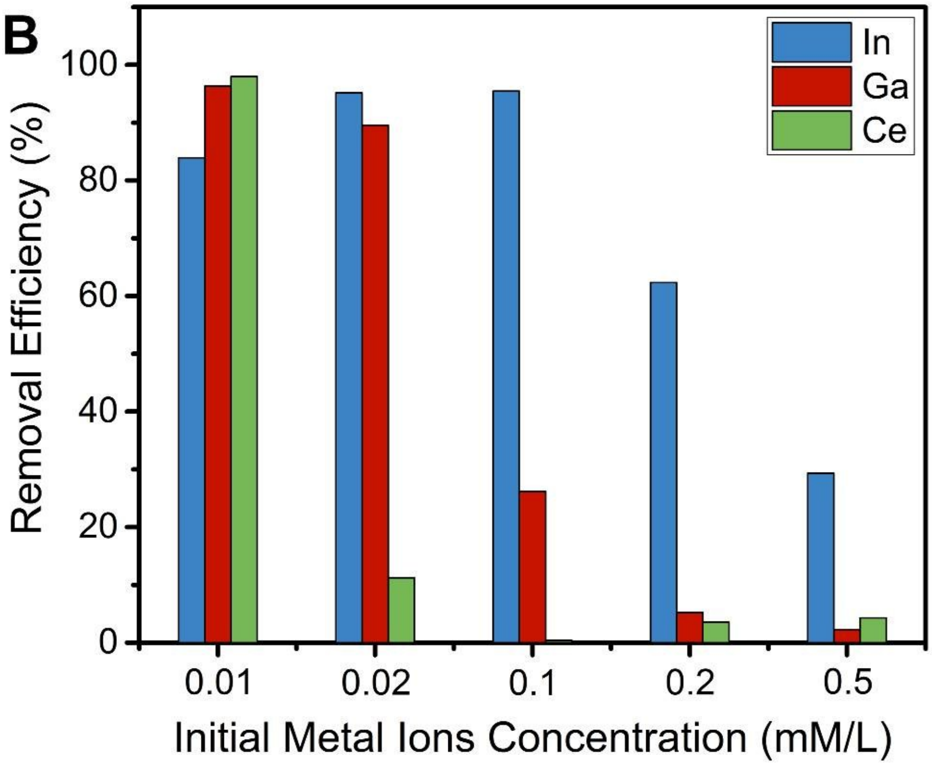
B
Removal Efficiency (%)
0
20
40
60
80
100
0.01
0.02
0.1
0.2
0.5
Initial Metal Ions Concentration (mM/L)
In
Ga
Ce

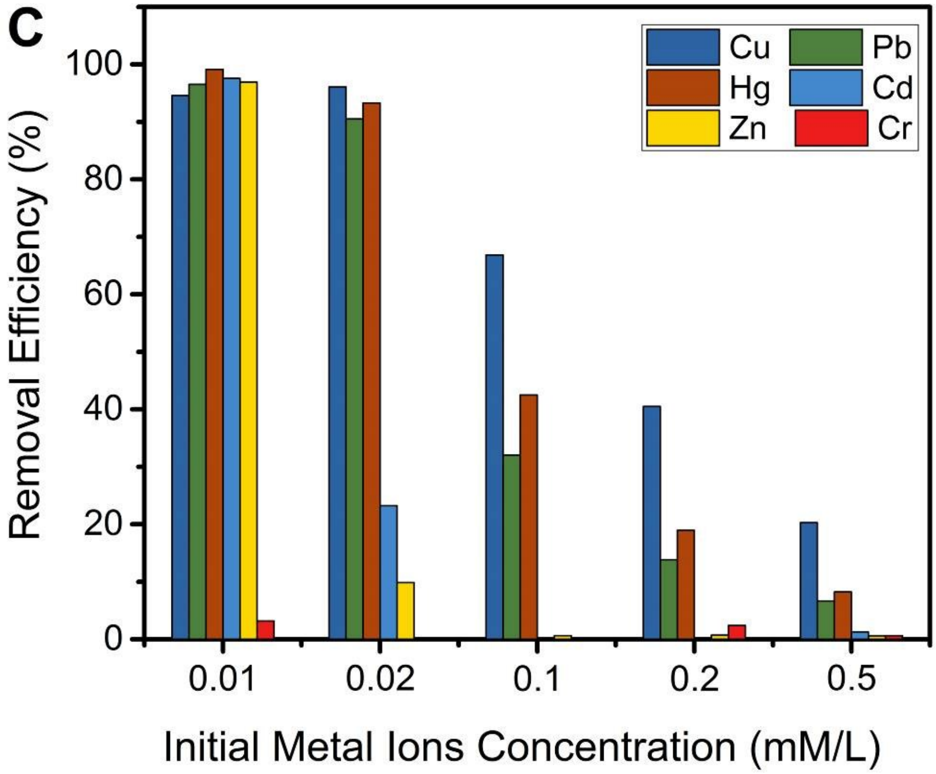
C
Removal Efficiency (%)
0
20
40
60
80
100
0.01
0.02
0.1
0.2
0.5
Initial Metal Ions Concentration (mM/L)
Cu
Pb
Hg
Cd
Zn
Cr

Figure S10. Equi-molar competitive sorption of multiple metal ions (A) Group 1: Cd^{2+} and Pb^{2+}; (B) Group 2: Ce^{3+}, In^{3+} and Ga^{3+}; and (C) Group 3: Cr^{3+}, Zn^{2+}, Cd^{2+}, Hg^{2+}, Pb^{2+} and Cu^{2+} onto Mag-Ligand at pH7 as a function of initial ions concentration with a fixed adsorbent concentration of 4 g/L.

References:

1. Y. Huang and A. A. Keller, *Water Research*, 2015, **80**, 159-168.
2. P. Wang, Q. Shi, Y. Shi, K. K. Clark, G. D. Stucky and A. A. Keller, *Journal of the American Chemical Society*, 2008, **131**, 182-188.
3. W. W. Wendlandt, *Anal Chem*, 1960, **32**, 848-850.
4. F. M. M. Morel and J. G. Hering, *Principles and Applications of Aquatic Chemistry*, Wiley, 1993.
5. N. T. Coleman, A. C. Mcclung and D. P. Moore, *Science*, 1956, **123**, 330-331.
6. J. P. Gustafsson, *Capturado em de*, 2006, **26**.
7. G. Issabayeva, M. K. Aroua and N. M. N. Sulaiman, *Bioresource Technol*, 2006, **97**, 2350-2355.
8. D. C. Harris, *Quantitative chemical analysis*, Macmillan, 2010.
9. M. C. Yappert and D. B. DuPre, *J Chem Educ*, 1997, **74**, 1422-1423.